Available online at www.sciencedirect.com
SCIENCE DIRECT®
Journal of Solid State Chemistry 178 (2005) 3639–3647
JOURNAL OF SOLID STATE CHEMISTRY
www.elsevier.com/locate/jssc

$PrCo_2Al_8$ and $Pr_2Co_6Al_{19}$: Crystal structure and electronic properties

O. Tougait[a,*], D. Kaczorowski[b], H. Noël[a]

[a]*Laboratoire de Chimie du Solide et Inorganique Moléculaire, Université de Rennes1, LCSIM, UMR CNRS 6511, 263 avenue du Général Leclerc, 35042 Rennes, France*
[b]*Institute of Low Temperature and Structure Research, Polish Academy of Sciences, P.O. Box 1410, 50-950 Wrocław, Poland*

Received 13 July 2005; received in revised form 7 September 2005; accepted 11 September 2005
Available online 12 October 2005

Abstract

The praseodymium cobalt aluminides, $PrCo_2Al_8$ and $Pr_2Co_6Al_{19}$, were prepared by reaction of the elemental components in an arc-melting furnace, followed by heat treatment at 900 °C for several days. Their chemical composition was checked by scanning electron microscopy and energy dispersive spectroscopy, and their crystal structure was refined from single crystal X-ray diffraction data. $PrCo_2Al_8$ adopts the $CaCo_2Al_8$ type of structure, crystallizing with the orthorhombic space group *Pbam*, with four formula units in a cell of dimensions at room temperature: $a = 12.4623(3)$ Å, $b = 14.3700(4)$ Å, $c = 4.0117(1)$ Å. $Pr_2Co_6Al_{19}$ crystallizes in the monoclinic space group *C2/m*, with four formula units in a cell of dimensions at room temperature: $a = 17.6031(4)$ Å, $b = 12.1052(4)$ Å, $c = 8.2399(2)$ Å and $\beta = 103.903(1)^\circ$. Its structure belongs to the $U_2Co_6Al_{19}$ type. The crystal structures of both compounds studied can be viewed as three-dimensional structures resulting from the packing of Al polyhedra centred by the transition elements. Along the *c*-axis, the coordination polyhedra around the Pr atoms pack by face sharing to form strands, which are separated one from another by an extended Co–Al network. Magnetic measurements have revealed that $PrCo_2Al_8$ orders antiferromagnetically at $T_N = 5$ K, with a clear metamagnetic transition occurring at a critical field $H_c = 0.9(1)$ T. The temperature dependence of the susceptibility of $Pr_2Co_6Al_{19}$ does not provide any evidence for long-range magnetic ordering in the temperature domain 1.7–300 K. At low temperatures ($T < 10$ K), the susceptibility saturates in a manner characteristic of a non-magnetic singlet ground state. At high temperatures, the magnetic susceptibility of each compound follows a Curie–Weiss law, with the effective magnetic moment per Pr atom of $3.48(5)\mu_B$ and $3.41(2)\mu_B$ for $PrCo_2Al_8$ and $Pr_2Co_6Al_{19}$, respectively. These values are close to the theoretical value of $3.58\mu_B$ expected for a free Pr^{3+} ion and exclude any contribution due to the Co atoms. Both compounds exhibit in the temperature range 5–300 K metallic-like electrical conductivity, and their Seebeck coefficient is of the order of several μV/K.

Keywords: Single-crystal X-ray diffraction; Magnetic susceptibility; Electrical resistivity; Seebeck coefficient; Heavy-fermions; Rare-earth intermetallics

1. Introduction

In intermetallic compounds based on *f*-elements having particular electronic configuration, the interaction between the unstable *f*-electrons and the conduction electrons may yield formation at low temperatures of heavy fermion ground state. A large number of Ce- or U-based intermetallics have been characterized as heavy-fermion systems, much less among Yb-based compounds and to our best knowledge, only three examples of such systems have been reported so far for Pr-based compounds, i.e. $PrInAg_2$ [1], $PrFe_4P_{12}$ [2] and $PrOs_4Sb_{12}$ [3], the latter phase also being a superconductor below $T_c = 1.85$ K. The recent findings of interesting physical properties of so-called filled skutterudite compounds, which are also promising candidates for novel thermoelectric materials, have renewed the interest in synthesis and characterization of the electronic properties of other Pr-based intermetallics. It is thought that the key mechanism leading to the anomalous behaviour observed in these materials is related to the interplay between quadrupolar interactions in a crystalline electrical field with the conduction electrons [4]. Therefore, the local symmetry and the coordination sphere around the Pr ions, which govern the ground-state properties, have to be considered of prime importance.

*Corresponding author. Fax: +33 2 23 23 67 99.
E-mail address: tougait@univ-rennes1.fr (O. Tougait).

0022-4596/$ - see front matter © 2005 Elsevier Inc. All rights reserved.
doi:10.1016/j.jssc.2005.09.019

Two series of compounds having structures with *f*-atoms inserted in a tri-dimensional framework, previously found in the course of our studies of rare-earth or actinide cobalt ternary aluminides compounds [5,6], were successfully extended to Pr. For these compounds, $PrCo_2Al_8$ and $Pr_2Co_6Al_{19}$, strong hybridization effects between the localized 4*f* electrons and conduction electrons provided by the Co–Al framework is expected. In the present paper, we report on the synthesis, structural analyses as well as on the electronic properties of these two compounds, studied by means of magnetic susceptibility, magnetization, resistivity and thermopower measurements.

2. Experimental section

2.1. Syntheses

Samples were prepared by reaction of the elements melted in an arc-furnace under argon atmosphere. The cooled buttons were flipped over and remelted three times to achieve good homogeneity. The weight losses were less than 1 wt%. Each sample was then placed into an alumina crucible and sealed in a fused silica tube under a residual atmosphere of argon. They were then heat treated at 900 °C for a period ranging from 150 up to 300 h.

2.2. Metallographic and chemical analyses

Metallographic and quantitative analyses were obtained with the use of a 6400-JSM scanning electron microscope equipped with an Oxford Link Isis spectrometer. The specimen prepared by embedding a piece of each sample in resin was thoroughly polished down to 1 μm. A thin layer of gold was deposited on the surface before metallographic analyses. The compounds $PrAl_2$, $PrCo_2$ and Co_2Al_5 were used as standards to superimpose additional corrections to the internal corrections for atomic number, absorption and fluorescence (ZAF-type corrections).

2.3. X-ray diffraction studies

All samples were analysed by powder X-ray diffraction patterns collected on an INEL CPS 120 diffractometer using a monchromatized Cu$K\alpha_1$ radiation. Comparison of the diffraction patterns with various types of structures was carried out with the help of the program POWDERCELL [7].

Single-crystal X-ray diffraction experiments were carried out at room temperature, with the use of a Nonius Kappa CCD diffractometer equipped with a Mo$K\alpha$ radiation. The unit-cell parameters, orientation matrix as well as the crystal quality were derived from 10 frames recorded at $\phi = 0$ using a scan of 1° in ω. The complete strategy to fill more than a hemisphere was automatically calculated with the use of the program COLLECT [8]. Data reduction and reflection indexing were performed with the program DENZO of the Kappa CCD software package [8]. The scaling and merging of redundant measurements of the different data sets as well as the cell refinement was performed using DENZO. Numerical or semi-empirical absorption corrections were made with the use of the programs ANALYTICAL [9] and MULTISCAN [10], respectively. All structure refinements and Fourier syntheses were carried out with the help of SHELXL-97 [11]. The atomic positions were standardized using STIDY [12]. The representations of the crystal structures were drawn with the help of DIAMOND 2.1 [13].

2.4. Measurements of physical properties

DC magnetic measurements were carried out using a Quantum Design MPMS-5 SQUID magnetometer. Zero field cooled (ZFC) and field cooled (FC) data were collected in the temperature range 1.7–350 K with applied fields of 0.1 and 0.5 T for $PrCo_2Al_8$ and $Pr_2Co_6Al_{19}$, respectively. The magnetization of both samples was measured at 1.7 K in increasing and decreasing magnetic fields up to 5 T.

The electrical resistivity was measured over the temperature interval 3.8–290 K employing the standard 4-probe DC technique. The electrical contacts to bar-shaped samples cut from the annealed ingots were made by indium soldering. The Seebeck coefficient was measured in the temperature range from 8 to 300 K, by standard differential method using copper as a reference material.

3. Results

3.1. Chemical and structural characterization

Based on powder diffraction experiments, $PrCo_2Al_8$ was reported to adopt the $CaCo_2Al_8$ type of structure with the lattice parameters $a = 12.37$ Å, $b = 14.43$ Å and $c = 4.01$ Å [14]. Our present structural investigation using single crystal X-ray diffraction techniques readily confirms the previous results. Table 1 summarizes the crystallographic details. Tables 2 and 3 give the atomic coordinates together with equivalent atomic displacement parameters and selected interatomic distances, respectively. X-ray powder diffraction and metallographic analyses revealed that $PrCo_2Al_8$ is a well-defined compound. Pure samples can be prepared by melting the constituents taken in the stoichiometric ratio, followed by a heat treatment at 900 °C for 150 h.

Initial investigations on the ternary compound $Pr_2Co_6Al_{19}$ were undertaken in analogy to the recently reported characterization of $U_2Co_6Al_{19}$ [15] and $Ce_2Co_6Al_{19}$ [6]. A sample with the initial composition $Pr_2Co_6Al_{19}$ was prepared and annealed at 900 °C for 300 h. X-ray powder diffraction and scanning electron microscopy–energy dispersive spectroscopy (SEM–EDS) analyses readily confirmed the existence of this new phase, which appeared as a single phase in this sample. The composition analysis did not reveal any significant

Table 1
Crystal data and structure refinements of $PrCo_2Al_8$ and $Pr_2Co_6Al_{19}$

Empirical formula	$PrCo_2Al_8$	$Pr_2Co_6Al_{18.94}$
Formula weight ($g\,mol^{-1}$)	474.6	1148.02
Crystal system, space group	Orthorhombic, *Pbam* (# 55)	Monoclinic, *C*2/*m* (# 12)
Unit cell dimensions (Å, deg)	$a = 12.4623(3)$ $b = 14.3700(4)$ $c = 4.0117(1)$	$a = 17.6031(4)$ $b = 12.1052(4)$, $c = 8.2399(2)$ $\beta = 103.903(1)$
Volume ($Å^3$)	718.4(1)	1704.4(1)
Z, Calculated density (g/cm^3)	4, 4.39	4, 4.49
Absorption coefficient (cm^{-1})	121	123
Crystal colour and habit	Black, plate like	Black, irregular prism
Crystal size (mm^3)	$0.09 \times 0.07 \times 0.03$	$0.08 \times 0.06 \times 0.04$
Theta range for data collection (deg)	2.16–41.13	3.89–44.93
Limiting indices	$-21 \leqslant h \leqslant 23$, $-19 \leqslant k \leqslant 26$, $-7 \leqslant l \leqslant 5$	$-34 \leqslant h \leqslant 34$, $-24 \leqslant k \leqslant 23$, $-15 \leqslant l \leqslant 16$
Reflections collected/unique	19045/2630	23716/7195
R (int)	0.083	0.077
Absorption correction	Analytical	Semi-empirical from equivalents
Max./min. transmission	0.5846/0.4582	0.5753/0.3456
Data/restraints/parameters	2630/0/70	7195/0/143
Goodness-of-fit on F^2	1.12	1.08
R indices $[I > 2\sigma(I)]$[a]	$R_1 = 0.042$, $wR_2 = 0.100$	$R_1 = 0.051$, $wR_2 = 0.096$
Extinction coefficient	0.0006(4)	0.00003(5)
Largest diff. peak and hole ($e\,Å^{-3}$)	7.79 and −3.144	6.292 and −4.418

$wR_2 = \left[\Sigma w(F_o^2 - F_c^2)^2 / wF_o^4\right]^{1/2}$, where $w^{-1} = [\sigma^2(F_o^2) + 7.27\,P]$, $P = [\max(F_o^2, 0) + 2F_c^2]/3$.
[a] $R(F) = \Sigma||F0| - |F_C||/|F_C|$.

Table 2
Atomic coordinates and equivalent isotropic displacement parameters ($Å^2$) for $PrCo_2Al_8$

Atom	Wyckoff position	*x*	*y*	*z*	$U_{eq.}$ ($Å^2$)
Pr	4*g*	0.340528(15)	0.318419(16)	0	0.01061(7)
Co(1)	4*g*	0.03468(4)	0.40576(4)	0	0.00958(10)
Co(2)	4*g*	0.15176(4)	0.09640(4)	0	0.00755(10)
Al(1)	4*h*	0.02516(10)	0.13181(9)	1/2	0.0093(2)
Al(2)	4*h*	0.16020(8)	0.37903(10)	1/2	0.0092(2)
Al(3)	4*h*	0.23640(10)	0.17293(9)	1/2	0.0102(2)
Al(4)	4*h*	0.33173(9)	0.49113(9)	1/2	0.0098(2)
Al(5)	4*h*	0.45252(10)	0.18003(8)	1/2	0.0097(2)
Al(6)	4*g*	0.09588(9)	0.25307(8)	0	0.0100(2)
Al(7)	4*g*	0.34020(8)	0.04453(10)	0	0.0107(2)
Al(8)	2*d*	0	1/2	1/2	0.0092(3)
Al(9)	2*a*	0	0	0	0.0103(3)

U_{eq} is defined as one-third of the trace of the orthogonalized U_{ij} tensor.

departure from the ideal stoichiometry. A tiny fragment of this sample was used for the single crystal X-ray diffraction study. The atomic positions from $U_2Co_6Al_{19}$ were taken as an initial structural model for the crystallographic refinement. At the first stage of the refinement, the displacement ellipsoids for the Al(1) and Al(4) atoms located on 4*g* and 8*j* Wyckoff positions were abnormally large and highly elongated along the *c*-direction, thus suggesting partial occupancy of these two Al sites. Consequently, the multiplicity of these positions along with the variable displacement parameters were allowed to vary, yielding the occupancies of 0.891(11) and 0.867(7) for Al(1) and Al(4), respectively. The difference Fourier map revealed residual peaks of about $5.5\,e\,Å^{-3}$, at a distance of less than 1 Å from the Al(1) and Al(4) sites. In subsequent refinements, the atomic parameters and the occupancy factors of these two additional sites were allowed to vary, whereas the isotropic displacement parameter was restricted to a reasonable value. The resulting occupancy factors were 0.097(5) and 0.077(4) for the atomic positions in the vicinity of Al(1) and Al(4), respectively. The sum of the occupancy factors over the two close atomic positions of each atom amounts to 0.90(2) and 0.98(1) for Al(1) and Al(4), respectively. We interpret these results as a partial delocalization of the Al(1) and Al(4) atoms over two crystallographic sites, indicating a small disorder within the structure. The chemical formula of $Pr_2Co_6Al_{18.94}$, deduced from the crystallographic refinement is in good agreement with the SEM–EDS analyses. The non-stoichiometry of $Pr_2Co_6Al_{19}$ which may be deemed to 1 at% of aluminium, is within the detection limit of our method of analysis. All relevant crystallographic details are listed in Table 1. Only the main

Table 3
Selected interatomic distances (Å) for $PrCo_2Al_8$

Pr–Al(1) × 2	3.135(1)	Co(1)–Al(6)	2.323(2)	Co(2)–Al(9)	2.344(1)
Pr–Al(2) × 2	3.136(1)	Co(1)–Al(8) × 2	2.459(1)	Co(2)–Al(6)	2.357(2)
Pr–Al(5) × 2	3.151(1)	Co(1)–Al(7)	2.527(2)	Co(2)–Al(7)	2.464(2)
Pr–Al(3) × 2	3.175(1)	Co(1)–Al(7)	2.531(2)	Co(2)–Al(3) × 2	2.519(1)
Pr–Al(6)	3.190(2)	Co(1)–Al(5) × 2	2.567(1)	Co(2)–Al(4) × 2	2.521(1)
Pr–Al(4) × 2	3.193(2)	Co(1)–Al(2) × 2	2.573(1)	Co(2)–Al(1) × 2	2.602(1)
Pr–Al(9)	3.280(1)	Co(1)–Co(1)	2.843(1)		
Pr–Al(6)	3.344(2)				
Al(1)–Co(3) × 2	2.331(1)	Al(2)–Al(8)	2.647(2)	Al(3)–Al(5)	2.695(2)
Al(1)–Al(4)	2.696(2)	Al(2)–Al(4)	2.677(2)	Al(3)–Al(1)	2.698(2)
Al(1)–Al(3)	2.698(2)	Al(2)–Al(5)	2.724(2)	Al(3)–Al(4)	2.747(2)
Al(1)–Al(9) × 2	2.777(1)	Al(2)–Al(6) × 2	2.818(2)		
Al(1)–Al(6) × 2	2.799(2)				
Al(1)–Al(5)	2.851(2)				
Al(4)–Al(2)	2.677(2)	Al(5)–Al(8)	2.654(2)	Al(6)–Al(1) × 2	2.799(2)
Al(4)–Al(1)	2.696(2)	Al(5)–Al(3)	2.695(2)	Al(6)–Al(2) × 2	2.818(2)
Al(4)–Al(3)	2.747(2)	Al(5)–Al(2)	2.724(2)	Al(6)–Al(5) × 2	2.853(2)
		Al(5)–Al(1)	2.851(2)		
Al(8)–Al(2) × 2	2.647(2)	Al(5)–Al(6) × 2	2.853(2)	Al(7)–Al(8) × 2	2.898(1)
Al(8)–Al(5) × 2	2.654(2)				
Al(8)–Al(7) × 4	2.898(1)	Al(9) Al(1) × 4	2.777(1)		

Only the Al–Al distances shorter than 2.90 Å are listed.

Table 4
Atomic coordinates and equivalent isotropic displacement parameters (Å^2) for $Pr_2Co_6Al_{19}$

Atom	Wyckoff position	x	y	z	$U_{eq.}$ (Å^2)
Pr(1)	4*i*	0.279421(15)	0	0.25743(3)	0.00739(6)
Pr(2)	4*i*	0.719883(15)	0	0.22828(3)	0.00746(6)
Co(1)	4*i*	0.43811(4)	0	0.09396(8)	0.00580(12)
Co(2)	4*i*	0.56164(4)	0	0.40555(8)	0.00565(12)
Co(3)	8*j*	0.11996(3)	0.19918(4)	0.18895(6)	0.00598(9)
Co(4)	8*j*	0.38374(3)	0.30156(4)	0.32608(6)	0.00727(9)
Al(1)[a]	4*g*	0	0.1692(2)	0	0.0228(10)
Al(2)	4*i*	0.08157(10)	0	0.6477(2)	0.0128(3)
Al(3)	4*i*	0.08628(10)	0	0.1820(2)	0.0123(3)
Al(4)[b]	8*j*	0.02584(8)	0.17439(14)	0.3649(2)	0.0164(4)
Al(5)	8*j*	0.05232(6)	0.38264(10)	0.15482(14)	0.0074(2)
Al(6)	8*j*	0.14688(7)	0.33187(11)	0.44799(14)	0.0091(2)
Al(7)	8*j*	0.17984(7)	0.11632(11)	0.46523(14)	0.0102(2)
Al(8)	8*j*	0.25174(6)	0.25063(11)	0.23826(14)	0.0111(2)
Al(9)	8*j*	0.33678(8)	0.38749(11)	0.04698(15)	0.0128(2)
Al(10)	8*j*	0.36249(7)	0.17484(11)	0.05610(14)	0.0106(2)
Al(11)	8*j*	0.44614(6)	0.11643(10)	0.35117(14)	0.0072(2)

[a]Occupancy of 0.891(11) and 0.867(7) for Al(1) and Al(4) respectively.
[b]The sum over the two sites amounts to 0.90(2) and 0.98(1) for Al(1) and Al(4), respectively.

occupied position for Al(1) and Al(4) has been considered in Tables 4 and 5, which present the final atomic parameters and a selection of interatomic distances, respectively. The rather large value of the atomic displacement parameters of Al(1) may be explained by geometric considerations (see below).

3.2. Crystal structure description

The crystal structures of $PrCo_2Al_8$ and $Pr_2Co_6Al_{19}$ are shown in Figs. 1 and 2, respectively. Both of them are close-packed structures resulting from the three-dimensional packing of Al polyhedra, centred by the transition elements. These coordination polyhedra pack by face-sharing to form strands parallel to the shortest axis (*c*-axis). For both structures, the strands containing Pr atoms are well separated from each other by an extended Co–Al network. It results that the shortest Pr–Pr contacts are found within the strands containing the rare-earth atoms.

The unique Pr atom per asymmetric unit of $PrCo_2Al_8$ is located in a distorted pentagonal prism, which has three of its rectangular faces additionally capped by an Al atom

Table 5
Selected interatomic distances (Å) for $Pr_2Co_6Al_{19}$

Pr(1)–Al(7) × 2	3.071(2)	Pr(2)–Al(7) × 2	3.055(2)	Co(1)–Al(5) × 2	2.414(2)
Pr(1)–Al(8) × 2	3.071(2)	Pr(2)–Al(8) × 2	3.068(2)	Co(1)–Al(10) × 2	2.480(2)
Pr(1)–Al(9) × 2	3.141(2)	Pr(2)–Al(9) × 2	3.130(2)	Co(1)–Al(11) × 2	2.521(2)
Pr(1)–Al(11) × 2	3.179(2)	Pr(2)–Al(6) × 2	3.192(2)	Co(1)–Al(5) × 2	2.533(2)
Pr(1)–Al(6) × 2	3.194(2)	Pr(2)–Al(5) × 2	3.198(1)		
Pr(1)–Al(10) × 2	3.246(2)	Pr(2)–Al(10) × 2	3.231(2)		
Pr(1)–Al(3)	3.306(2)	Pr(2)–Al(2)	3.398(2)		
Co(2)–Al(11) × 2	2.425(2)	Co(3)–Al(1)	2.331(1)	Co(4)–Al(8)	2.344(2)
Co(2)–Al(11) × 2	2.480(2)	Co(3)–Al(8)	2.341(2)	Co(4)–Al(4)	2.462(2)
Co(2)–Al(5) × 2	2.481(2)	Co(3)–Al(4)	2.468(2)	Co(4)–Al(7)	2.474(2)
Co(2)–Al(6) × 2	2.503(2)	Co(3)–Al(7)	2.479(2)	Co(4)–Al(2)	2.475(1)
		Co(3)–Al(3)	2.480(1)	Co(4)–Al(9)	2.478(2)
Al(1)–Al(3) × 2	2.767(2)	Co(3)–Al(9)	2.484(2)	Co(4)–Al(11)	2.482(2)
		Co(3)–Al(5)	2.504(2)	Co(4)–Al(6)	2.617(2)
Al(2)–Al(4) × 2	2.819(2)	Co(3)–Al(10)	2.607(2)	Co(4)–Al(10)	2.654(2)
		Co(3)–Al(6)	2.622(2)	Co(4)–Al(4)	2.675(2)
Al(3)–Al(1) × 2	2.767(2)	Al(4)–Al(4)	2.600(3)	Al(5)–Al(10)	2.647(2)
Al(3)–Al(7) × 2	2.880(2)	Al(4)–Al(7)	2.729(2)	Al(5)–Al(6)	2.656(2)
		Al(4)–Al(6)	2.818(2)	Al(5)–Al(11)	2.750(2)
		Al(4)–Al(2)	2.819(2)	Al(5)–Al(5)	2.765(2)
		Al(4)–Al(11)	2.884(2)	Al(5)–Al(5)	2.841(2)
Al(6)–Al(11)	2.667(2)	Al(7)–Co(4)	2.474(2)	Al(8)–Al(10)	2.882(2)
Al(6)–Al(7)	2.669(2)	Al(7)–Al(7)	2.816(3)	Al(8)–Al(10)	2.898(2)
Al(9)–Co(3)	2.484(2)	Al(10)–Al(11)	2.619(2)	Al(11)–Al(6)	2.667(2)
Al(9)–Al(10)	2.612(2)	Al(10)–Al(5)	2.647(2)	Al(11)–Al(11)	2.716(2)
Al(9)–Al(9)	2.724(3)	Al(10)–Al(1)3	2.670(2)	Al(11)–Al(5)	2.750(2)
		Al(10)–Al(8)	2.898(2)	Al(11)–Al(11)	2.819(2)
				Al(11)–Al(4)	2.884(2)

Only the Al–Al distances shorter than 2.90 Å are listed.

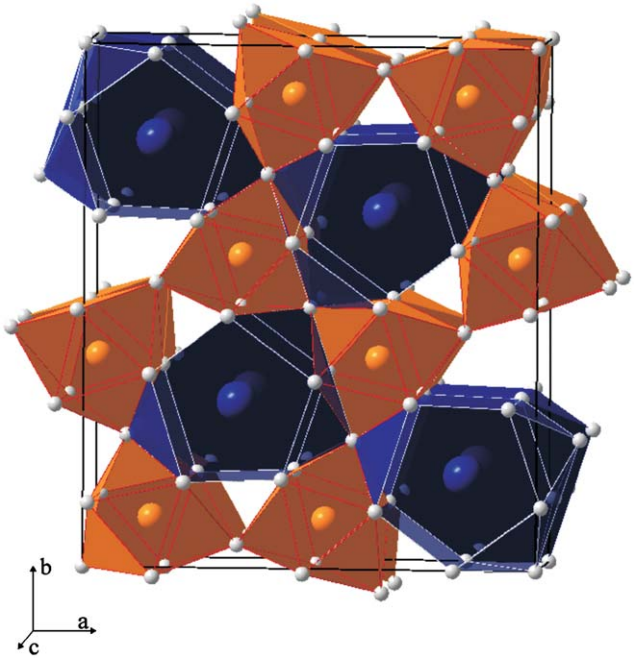

Fig. 1. Crystal structure of $PrCo_2Al_8$ viewed down the *c*-axis. The polyhedra of Al around the Pr and Co atoms are drawn in blue/dark grey and orange/light grey, respectively.

(see Fig. 3a). Along the *c*-axis the prisms share their pentagonal faces, giving Pr–Pr separation of 4.012(1) Å. The Pr–Al interatomic distances range from 3.1352(9) to 3.344(2) Å. With the exception of the distances Pr–Al(9) of 3.280(1) and Pr–Al(6) of 3.344(2) Å, which correspond to the separation of the central atom from the capping atom, they are shorter than the sum of the metallic radii of Pr (1.82 Å) and Al (1.43 Å). The two crystallographically non-equivalent Co atoms occupy tricapped trigonal prisms. Along the *c*-axis, both types of prisms are linked by sharing their triangular faces. Onto the *ab*-plane, two adjacent Co(1)Al9 prisms are connected by corner-sharing, whereas two adjacent Co(2)Al9 prisms are connected by edge-sharing. The connection between the two types of trigonal prisms centred by the Co atoms occurs by corner-sharing. The Co–Al interatomic distances in the Co(1)Al9 and Co(2)Al9 trigonal prisms range from 2.323(2) to 2.602(1) Å. These values are smaller than the sums of the metallic radii of Co (1.25 Å) and Al (1.43 Å), yet correspond well with the distances observed in the binary Co_2Al_9 [16]. Similarly, a large number of Al–Al interatomic distances in $PrCo_2Al_8$ are shorter than the sum of the metallic radii of Al but are consistent with the experimental values reported for binary and ternary aluminides [15–20].

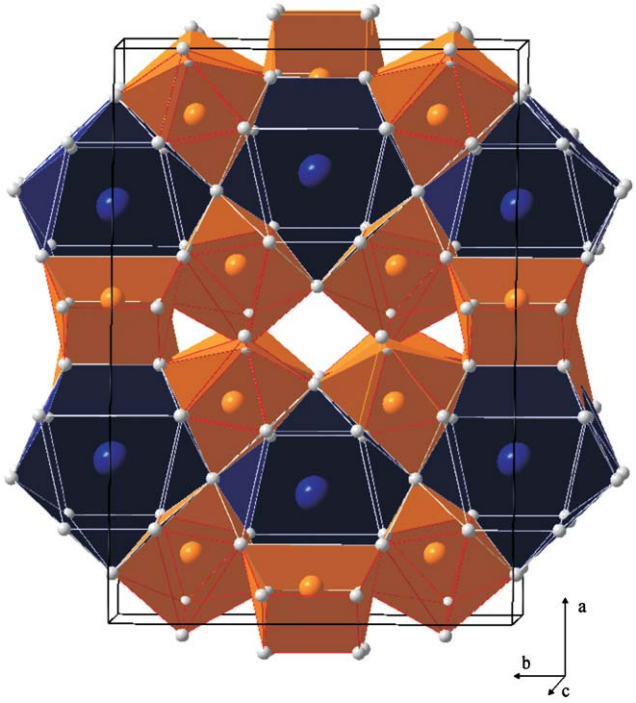

Fig. 2. Crystal structure of $Pr_2Co_6Al_{19}$ viewed down the *c*-axis. The polyhedra of Al around the Pr and Co atoms are drawn in blue/dark grey and orange/light grey, respectively.

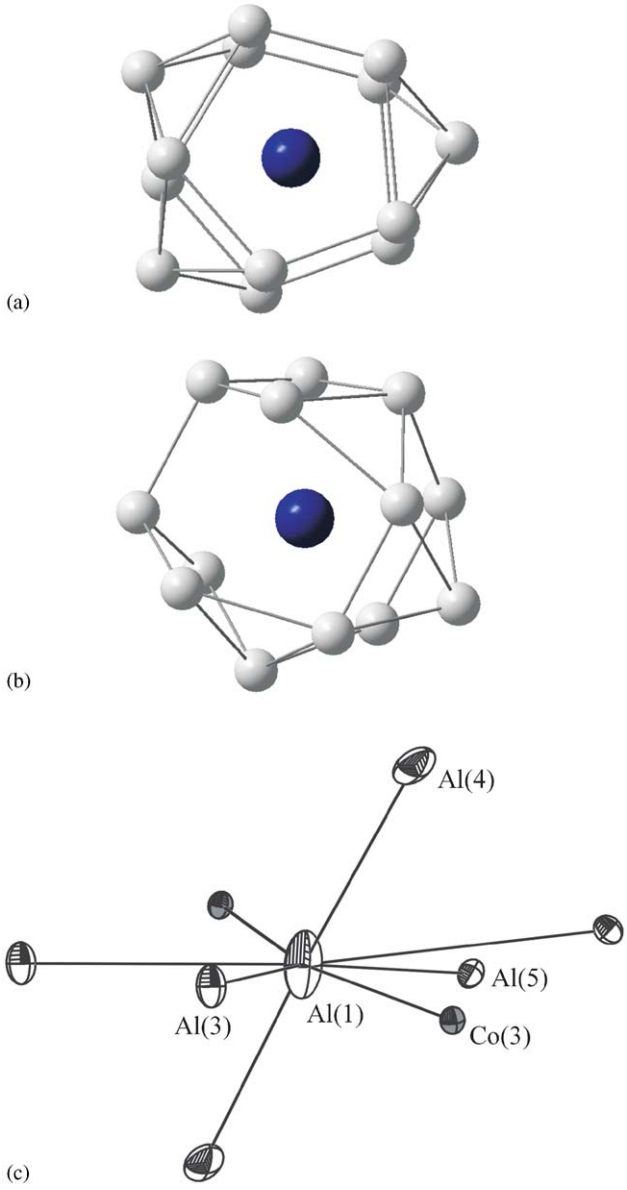

Fig. 3. The coordination geometries of (a) Pr atom in $PrCo_2Al_8$, (b) Pr(1) atom in $Pr_2Co_6Al_{19}$, with only the Al–Al bonds shorter than 2.90 drawn and (c) Al(1) in $Pr_2Co_6Al_{19}$. Displacement ellipsoids in panel (c) are drawn at the 50% probability level.

The two crystallographically independent Pr atoms per unit-cell of $Pr_2Co_6Al_{19}$ are coordinated by 13 Al atoms with a geometry that is derived from a cubooctahedron. Such a motif may be viewed as a cubooctahedron having one apex split into two positions (Fig. 3b). Along the *c*-direction, these coordination polyhedra pack by face-sharing, yielding two alternating Pr–Pr distances of 4.000(1) and 4.232(1) Å. The Pr–Al interatomic distances range from 3.055(2) to 3.398(2) Å. With the exception of one rather long contact for each non-equivalent Pr atom, Pr(1)–Al(3) of 3.306(2) Å and Pr(2)–Al(2) of 3.398(2) Å, all the other distances are shorter than 3.25 Å, calculated from the sum of the metallic radii of Pr and Al. The coordination spheres around the four Co sites in the unit cell of $Pr_2Co_6Al_{19}$ display two different geometries. The Co(1) and Co(2) atoms have a coordination of 8 Al atoms that form a distorted square prism. Such prisms are face-sharing along the *c*-axis to form a fluorite-like slab. In turn, the Co(3) and Co(4) atoms are surrounded by 9 Al atoms in a tricapped trigonal prismatic geometry. Onto the *ab*-plane, they pack by corner-sharing, so defining small octahedral cavities. The Co–Al interatomic distances are shorter than 2.68 Å, which is the sum of the metallic radii of Co and Al. As a consequence of high atomic content of Al, a large number of Al–Al contacts are found with distances below the sum of the metallic radii of Al (2.86 Å). With regard to the coordination of Al(1), it comprises a slightly staggered hexagon formed by 4 Al and 2 Co atoms, with rather short interatomic distances. The shape of the displacement ellipsoid and the partial delocalization of Al(1) can be understood as a tendency to move away from the plane of the hexagonal geometry of its environment (Fig. 3c).

To conclude this section, we note strong resemblances between the crystal structures of the two compounds investigated. Both $PrCo_2Al_8$ and $Pr_2Co_6Al_{19}$ can be described in terms of condensation by face-sharing of polyhedra centred by transition elements along the *c*-axis. Onto the *ab* plane these polyhedra are mainly connected by corner-sharing. The close examination of the interatomic distances revealed strong interactions in the pairs: Pr–Al, Co–Al and Al–Al. No bonding or at most extremely weak

interactions were found in the pairs of atoms: Pr–Co, Co–Co and Pr–Pr.

3.3. Magnetic properties

Fig. 4 shows the magnetic behaviour of $PrCo_2Al_8$. At low temperatures a pronounced maximum is observed in the thermal variation of the susceptibility (top-left insert) revealing that $PrCo_2Al_8$ orders antiferromagnetically at $T_N = 5$ K. In the magnetization process, a step-like metamagnetic transition occurs at a critical field, $H_c = 0.9(1)$ T (right-bottom insert), which corroborates the antiferromagnetic ground state. At 1.72 K, the nearly saturated magnetic moment amounts to $2.15\mu_B$/Pr atom, which is smaller than the value expected for a free Pr^{3+} ion ($gJ = 3.2$). This distinct reduction is a result of crystalline field effect.

In the paramagnetic state the magnetic susceptibility of $PrCo_2Al_8$ exhibits a Curie–Weiss behaviour only above 120 K. The effective magnetic moment $\mu_{eff} = 3.48(2)\mu_B$ per formula unit is very close to the moment expected for a free trivalent Pr ion ($g[J(J+1)]^{1/2} = 3.58$), thus indicating that exclusively Pr atoms carry magnetic moments, i.e. Co atoms are nonmagnetic. The positive value of the paramagnetic Weiss temperature $\Theta = 31(1)$ K likely manifests the presence of strong ferromagnetic exchange interactions in antiferromagnetic $PrCo_2Al_8$. At temperatures below 120 K, the inverse magnetic susceptibility strongly deviates from a straight-line behaviour, presumably because of gradual depopulation of excited crystalline field levels.

The thermal variation of the inverse magnetic susceptibility of $Pr_2Co_6Al_{19}$ is displayed in the main panel of Fig. 5. No evidence of any long-range magnetic ordering can be detected in the temperature domain 1.72–300 K. In line with this observation, the magnetization measured at 1.72 K with increasing and decreasing magnetic field is nearly proportional to the field strength (see the insert). Least-squares fitting of the susceptibility data taken in the temperature range 20–300 K to the Curie–Weiss law yield the effective magnetic moment $\mu_{eff} = 3.41(2)\mu_B$/Pr atom and the paramagnetic Curie temperature $\Theta = -11(1)$ K. Hence, the magnetic properties of $Pr_2Co_6Al_{19}$ are governed by localized magnetic moments of trivalent Pr ions, while Co atoms remain nonmagnetic. The relatively large negative value of Θ may signal some antiferromagnetic correlations. Below ca. 20 K, the $\chi^{-1}(T)$ curve departs from the Curie–Weiss law and at the lowest temperatures studied one observes a clear saturation of the magnetic susceptibility. Such a feature is characteristic of systems with singlet ground states, with a few representatives known amidst Pr-based compounds, PrP [21], $PrNi_5$ [22], $PrSn_3$ [23] and $PrRu_4Sb_{12}$ [24] as examples.

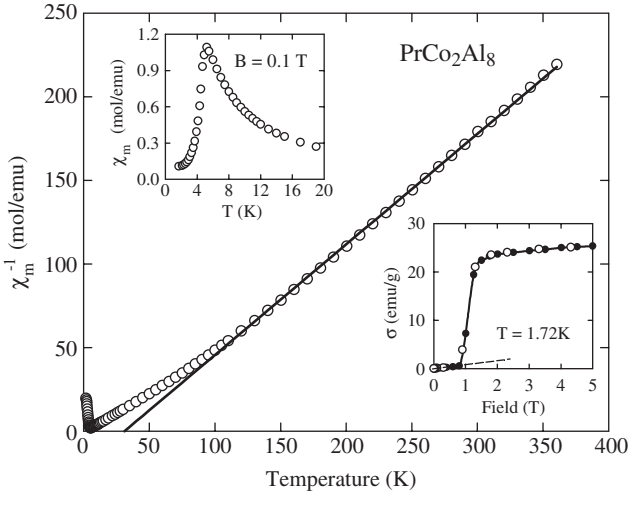

Fig. 4. Temperature dependence of the inverse magnetic susceptibility of $PrCo_2Al_8$ measured in a field of 0.1 T. The solid line represents the fit of the data to the Curie–Weiss law. The inset in the top-left corner presents the susceptibility measured at low temperatures. The inset in the bottom-right corner presents the field dependence of the magnetization recorded at 1.72 K with increasing (full circles) and decreasing (open circles) field. The dashed straight-line emphasizes the metamagnetic transition.

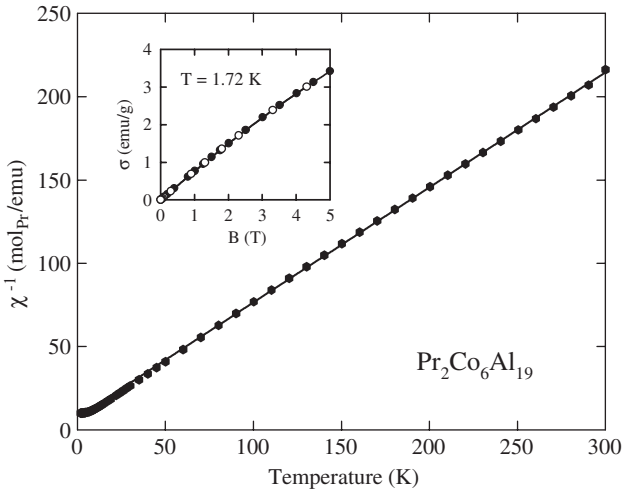

Fig. 5. Temperature dependence of the inverse magnetic susceptibility of $Pr_2Co_6Al_{19}$ measured in a field of 0.5 T. The solid line represents the fit of the data to the Curie–Weiss law. The inset presents the field dependence of the magnetization recorded at 1.72 K with increasing (full circles) and decreasing (open circles) field.

3.4. Electrical transport properties

Fig. 6 shows the temperature dependence of the electrical resistivity of $PrCo_2Al_8$. The compound exhibits metallic-like conductivity, yet with pronounced curvature of $\rho(T)$ in the entire paramagnetic region. The residual resistivity ratio RRR for the specimen measured is about 40. The value of the resistivity at room temperature is of the order 120 μΩ cm, it decreases with decreasing temperature to reach a plateau of about 12 μΩ cm below 20 K, and finally rapidly drops in the ordered state down to about 3 μΩ cm measured at 3.8 K. As shown in the inset to Fig. 6, the antiferromagnetic phase transition manifests itself as a distinct peak in the temperature derivative of the resistivity.

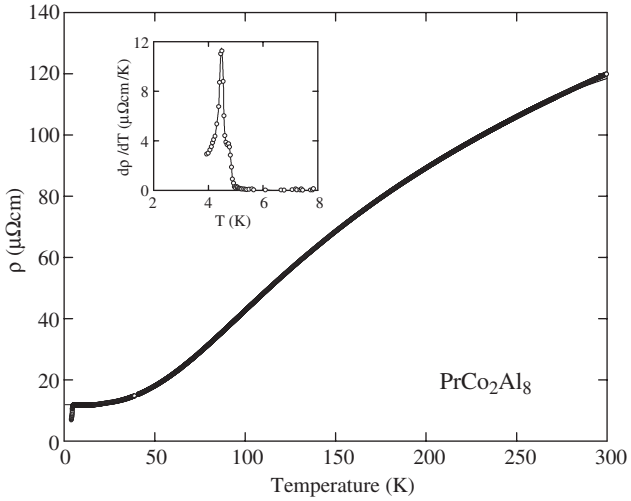

Fig. 6. Electrical resistivity of $PrCo_2Al_8$ as a function of temperature. The solid curve is a BGM fit described in the text. The inset presents the temperature derivative of the low-temperature resistivity.

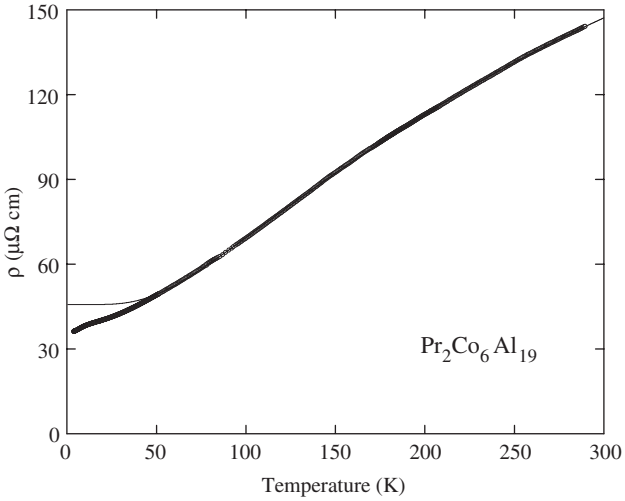

Fig. 7. Electrical resistivity of $Pr_2Co_6Al_{19}$ as a function of temperature. The solid curve is a BGM fit described in the text.

Interestingly, the sharp maximum in $d\rho/dT(T)$ is centred at 4.5 K, i.e. half a Kelvin below the Neel point derived from the magnetic data, whereas at $T_N = 5$ K there forms a step in the $d\rho/dT(T)$ peak. This behaviour may signal a subsequent order–order phase transition occurring in $PrCo_2Al_8$ just below T_N.

Assuming the validity of the Matthiessen rule, the resistivity of $PrCo_2Al_8$ may be described in the paramagnetic region by a so-called Bloch–Grüneissen–Mott (BGM) formula [25]:

$$\rho(T) = (\rho_0 + \rho_0^{\infty}) + 4RT\left(\frac{T}{\Theta_D}\right) \times^4 \int_0^{\Theta_D/T} \frac{x^5\,dx}{(e^x - 1)(1 - e^{-x})} - KT^3,$$

where $(\rho_0 + \rho_0^{\infty})$ stands for the sum of the residual resistivity due to static defects in the crystal lattice and the spin-disorder resistivity due to the presence of disordered magnetic moments, respectively, the second term describes the phonon contribution to the total resistivity, and the third one represents $s-d$ interband scattering processes. The solid line in Fig. 6 is a least-squares fit of the experimental $\rho(T)$ data to the above expression. The so-derived values of the sum $\rho_0 + \rho_0^{\infty}$, the Debye temperature Θ_D and the coefficients R and K are as follows: $\rho_0 + \rho_0^{\infty} = 11.8\,\mu\Omega\,cm$, $\Theta_D = 283$ K, $R = 0.483\,\mu\Omega\,cm/K$ and $K = 1.16 \times 10^{-6}\,\mu\Omega\,cm/K^3$. Worth noting is the high value of K, directly related to the curvature in $\rho(T)$, that signifies the importance of scattering of the conduction electrons via Mott-type processes.

The electrical resistivity of the other compound studied, i.e. $Pr_2Co_6Al_{19}$, exhibits a less curvilinear character (see Fig. 7). It is also metallic-like, with a room-temperature value of $144\,\mu\Omega\,cm$ and a value of about $36\,\mu\Omega\,cm$ measured at 3.8 K (RRR = 4). However, a quantitative analysis of $\rho(T)$ in terms of the BGM model is reasonable only above 50 K (note the solid line in Fig. 7), and yields the following values of the fit parameters: $\rho_0 + \rho_0^{\infty} = 45.7\,\mu\Omega\,cm$, $\Theta_D = 324$ K, $R = 0.414\,\mu\Omega\,cm/K$ and $K = 5.5 \times 10^{-7}\,\mu\Omega\,cm/K^3$. As expected, K is much lower than that estimated for $PrCo_2Al_8$, whereas the phonon contribution to the resistivity is in both compounds of a similar magnitude. Apparently, at the lowest temperatures measured the resistivity of $Pr_2Co_6Al_{19}$ does not follow the BGM model and this observation signals the significance of crystalline field effects, which are neglected in this approach. Below 10 K $\rho(T)$ shows a downward curvature that may be associated with depopulation of the excited crystal field states down to the singlet ground state encountered in the magnetic susceptibility study.

Fig. 8 displays the temperature variations of the thermoelectric power of $PrCo_2Al_8$ and $Pr_2Co_6Al_{19}$. In line with metallic character of both materials their thermopower is rather small, being of the order of several μV/K. For the former compound the Seebeck coefficient changes its sign from positive at low temperatures to negative above 156 K. In the case of $Pr_2Co_6Al_{19}$ it remains positive in the entire temperature range. At high temperatures $S(T)$ of both phases is roughly proportional to temperature as expected for the thermopower due to electron thermal diffusion [25]. In turn, broad humps seen on $S(T)$ may be interpreted as being caused by the so-called phonon-drag effect. The latter contribution increases at low temperatures as T^3 and changes as T^{-1} at higher temperatures, hence giving rise to the formation in $S(T)$ of a maximum that occurs at a temperature of $0.1-0.3\,\Theta_D$ [26]. For the compounds studied the Debye temperature Θ_D estimated from the resistivity data is about 300 K, which would indeed be consistent with the peak in $S(T)$ occurring near 50 K. Another possible mechanism that may give rise to the formation of the positive maxima in the thermopower of

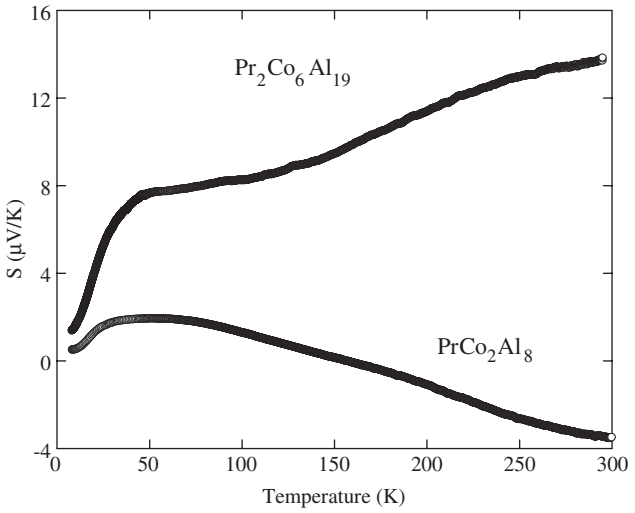

Fig. 8. Temperature dependencies of the thermoelectric power of $PrCo_2Al_8$ and $Pr_2Co_6Al_{19}$.

both $PrCo_2Al_8$ and $Pr_2Co_6Al_{19}$ is inelastic scattering of charge carriers by acoustic phonons [27].

Acknowledgments

The authors are grateful to D. Badurski and K. Gofryk for their assistance in electrical resistivity and thermoelectric power measurements, respectively. We acknowledge the use made of the Nonius Kappa CCD diffractometer through the Centre de Diffraction X de l'Université de Rennes1 (CDIFX). The work was supported by the Polish State Committee for Scientific Research (KBN) within Grant No. 4 T08A 04524.

References

[1] A. Yatskar, W.P. Beyermann, R. Movshovich, P.C. Canfield, Phys. Rev. Lett. 77 (1996) 3637–3640.
[2] H. Sato, Y. Abe, H. Okada, T.D. Matsuda, K. Abe, H. Sugawara, Y. Aoki, Phys. Rev. B 62 (2000) 15125–15130.
[3] E.D. Bauer, N.A. Frederick, P.-C. Ho, V.S. Zapf, M.B. Maple, Phys. Rev. B 65 (2002) 100506(R).
[4] H. Sugawara, T.D. Matsuda, K. Abe, Y. Aoki, H. Sato, S. Nojiri, Y. Inada, R. Settai, Y. Onuki, Phys. Rev. B 66 (2002) 134411–134415.
[5] H. Noël, O. Tougait, R. Troć, V.I. Zaremba, Solid State Sci. 7 (2005) 780–783.
[6] D. Kaczorowski, O. Tougait, A. Czopnik, Cz. Marucha, H. Noël, J. Magn. Magn Mater. 272–276 (2004) 239–241.
[7] W. Krause, G. Nolze, Federal Institute for Materials Research and Testing, Berlin, Germany.
[8] Nonius, In: Collect, Denzo, Scalepack, Sortav, Kappa CCD Program Package, Nonius BV, Delft, The Netherlands, 1998.
[9] J. de Meulenaar, H. Tompa, Acta Crystallogr. A 19 (1965) 1014.
[10] R.H. Blessing, Acta Crystallogr. A 51 (1995) 33.
[11] G.M. Sheldrick, SHELXS97 and SHELXL97, Program for Structure Solution and Refinement, University of Göttingen, Germany, 1997.
[12] E. Parthé, L. Gelato, B. Chabot, K. Cenzual, R. Gladyshevskii, TYPIX, Standardized data and crystal chemical characterization of inorganic structure types, Gmelin Handbook of Inorganic and Organometallic Chemistry, vol. 1, 8th ed., Springer, Berlin, 1993.
[13] G. Bergerhoff, DIAMOND, Gerhard-Domagkstraβe 1, 53121 Bonn, Germany 1996.
[14] R.M. Rykhal, O.C. Zarechnjuk, C.V. Protasov, Dopov. Akad. Nauk. Ukr. RSR Ser. A 47 (1985) 73–75.
[15] O. Tougait, J. Stępień-Damm, V. Zaremba, H. Noël, R. Troć, J. Solid State Chem. 174 (2003) 152–158.
[16] M. Boström, H. Rosner, Yu. Prots, U. Burkhardt, Yu. Grin, Z. Anorg. Allg. Chem. 631 (2005) 534–541.
[17] O. Tougait, H. Noël, Intermetallics 12 (2004) 219–223.
[18] R.E. Gladyshevskii, K. Cenzual, E. Parthé, J. Less Common Met. 182 (1992) 165–170.
[19] V.M.T. Thiede, W. Jeitschko, S. Niemann, T. Ebel, J. Alloy Compd. 267 (1998) 23–31.
[20] J. Stępień-Damm, O. Tougait, V.I. Zaremba, H. Noël, R. Troć, Acta Crystallogr. C 60 (2004) i7–i8.
[21] R.P. Guertin, L.D. Longinotti, E. Bucher, L. Kupferberg, S. Foner, Phys. Rev. B 12 (1975) 1005–1014.
[22] M. Reiffers, Y.G. Naidyuk, A.G.M. Jansen, P. Wyder, I.K. Yanson, D. Gignoux, D. Schmitt, Phys. Rev. Lett. 62 (1989) 1560–1563.
[23] A.I. Abou Aly, S. Bakanowski, N.F. Berk, J.E. Crow, T. Mihalisin, Phys. Rev. Lett. 35 (1975) 1387–1390.
[24] T. Hotta, Phys. Rev. Lett. 94 (2005) 067003 (1–4).
[25] N.F. Mott, H. Jones, The Theory of the Properties of Metals and Alloys, Oxford University Press, Oxford, 1958.
[26] F. Blatt, P. Schroeder, C. Foiles, D. Greig, Thermoelectric Power of Metals, Plenum, New York, 1976.
[27] K. Durczewski, M. Ausloos, Phys. Rev. B 49 (1994) 13215.